INSTITUT DE FRANCE
Académie des sciences

Comptes Rendus
Mécanique

Bachar Mallat, Gaele Perret, Gilles Godard and Denis Lebrun

Particles concentration and distribution over fixed rippled beds under waves by digital in-line holography

Volume 350 (2022), p. 309-323

Published online: 4 July 2022

https://doi.org/10.5802/crmeca.121

Les Comptes Rendus. Mécanique *sont membres du Centre Mersenne pour l'édition scientifique ouverte*
www.centre-mersenne.org
e-ISSN : 1873-7234

Comptes Rendus
Mécanique
2022, Vol. 350, p. 309-323
https://doi.org/10.5802/crmeca.121

Short paper / *Note*

Particles concentration and distribution over fixed rippled beds under waves by digital in-line holography

Bachar Mallat *, [a], **Gaele Perret** [a], **Gilles Godard** [b] and **Denis Lebrun** [b]

[a] UMR 6294 - LOMC, Normandie Université, CNRS, Université Le Havre Normandie, 76600, Le Havre, France

[b] UMR 6614 - CORIA, Normandie Université, CNRS, Université et INSA de Rouen, 76801, Saint-Etienne-du-Rouvray, France

E-mails: bachar.k.mallat@gmail.com (B. Mallat), gaele.perret@univ-lehavre.fr (G. Perret), gilles.godard@coria.fr (G. Godard), lebrun@coria.fr (D. Lebrun)

Abstract. Digital in-line holography (DIH) measurements are performed in a wave flume tank to study the three dimensional distribution of spherical Polyvincyl Chloride (PVC) particles over three fixed rippled beds under regular water waves. Homogeneous and heterogeneous particles in sizes are considered. The positions of PVC particles are reconstructed from holograms to assess their volume concentration and distribution during the decay of surface waves. Particles concentration and distribution are estimated close to the bottom in three zones: above ripple crest, above ripple trough and between them. 3D Particle trajectories in the vicinity of ripple crest and trough are studied during particles sedimentation. It is observed that distributions of fine particles are larger above troughs and their amplitudes of motion are larger than coarse particles, when they reach the rippled bed faster.

Keywords. Digital in-line holography, Morphodynamics, Sedimentation, Wave damping, Particle concentration, Ripple crest, Ripple trough.

Manuscript received 7 January 2022, revised 10 June 2022, accepted 13 June 2022.

1. Introduction

The complex interactions between water waves and a sedimentary bottom generates periodic patterns with typical wavelengths of few centimeters, which cover seabeds in coastal zones. These structures are called ripples. Their morphology affects sediment transport, wave damping, and boundary layer structure. Many studies are conducted considering the case of homogeneously sized grains [1, 2]. However, sediments are usually heterogeneous in size in coastal zones [3]. In such cases, their morphology varies with the organization of the sediments depending on

* Corresponding author.

grain sizes. The sediments used in these works range from fine (d_{50} = 0.25 mm) [4] to medium (d_{50} = 0.35 mm) [5] and coarse particles (d_{50} = 0.58 mm) [6].

Numerous studies deal with the deposit of particles on ripples as well as their concentrations above ripple crests [5, 7, 8]. Among others, in the studies of [9, 10], fine grains were observed to accumulate mostly along the ripple trough, while coarse sediments mostly accumulate along the ripple crests. Chu *et al.* [11] observed that fine particles concentrate on the top of ripple crests, while coarse particles settle more uniformly along the rippled bed. Lagrangian tracking of individual sediment grains combined with particle image velocimetry (PIV) measurements has been performed by [12] over a movable rippled bed. They observed that vortex ejection from the ripple crest during the accelerating phase of the flow cycle produced significantly larger quantities of suspended sediment transport.

On the other hand, numerical models have also been developed to assess the sediment transport over ripples under oscillatory flows [13–16]. The numerical results have shown that the hydrodynamics over ripples are influenced by vortex formation and ejection [14] and the wave energy dissipation is enhanced. Even if these models improve the understanding of small-scale bottom boundary layer processes, more detailed experiments are needed to validate these numerical models to assess sediment transport over ripples.

Nevertheless, if the techniques in literature provide details about the particle trajectories above rippled beds, they do not give information about the organisation of particle sedimentation from 3D perspective. For that purpose, a specific experimental protocol has been developed in a wave flume tank, allowing the characterization of particle sedimentation and deposit over a fixed rippled bed by digital in-line holography (DIH). With this optical technique, the 3D particle coordinates as well as the particle sizes can be measured.

The first part of this paper presents the experimental set-up allowing the study of particles motions above a rippled bed in a wave flume tank by digital in-line holography. The second part is devoted to the calibration to identify the optical magnification factor, essential for calculating 3D particle coordinates. The third part presents the results. The concentrations and distribution of heterogeneous particles are characterized in different zones during the wave damping. The 3D particles trajectories are then addressed above crest and trough. The use of holography in such configuration improves knowledge of the 3D particle motions above rippled beds under waves.

2. Materials and experimental methods

2.1. *Experimental set-up*

Experiments are carried out at LOMC (Laboratoire Ondes et Milieux Complexes) wave flume tank at the University of Le Havre Normandy in France. The wave flume tank dimensions are 10 m length × 0.3 m width × 0.3 m height. On one side a wave generator with one oscillating paddle generates regular waves with a frequency range between f = 0.6–1.6 Hz and a maximum height of 60 mm. On the other side, a porous beach reduces the reflection coefficient to less than 5%. The free surface elevation is measured by two wave probes. The water depth is fixed at h = 20 cm.

Three fixed rippled beds are considered (see Table 1). The bed profiles have been designed in steel, following the parametric relationships (1) [17]:

$$x = \zeta - \frac{H_r}{2}\sin\left(\frac{2\pi\zeta}{L_r}\right), \quad y = \frac{H_r}{2}\cos\left(\frac{2\pi\zeta}{L_r}\right) \tag{1}$$

where H_r is the ripple height, L_r is the wavelength of the ripples, ζ is a dummy variable, and x and y the distances measured in the horizontal and vertical directions respectively. Ripple geometrical characteristics are determined using Lebunetel's formula [18] for heterogeneous ripples at equilibrium state for deep sea wave conditions. The expression of the amplitude is

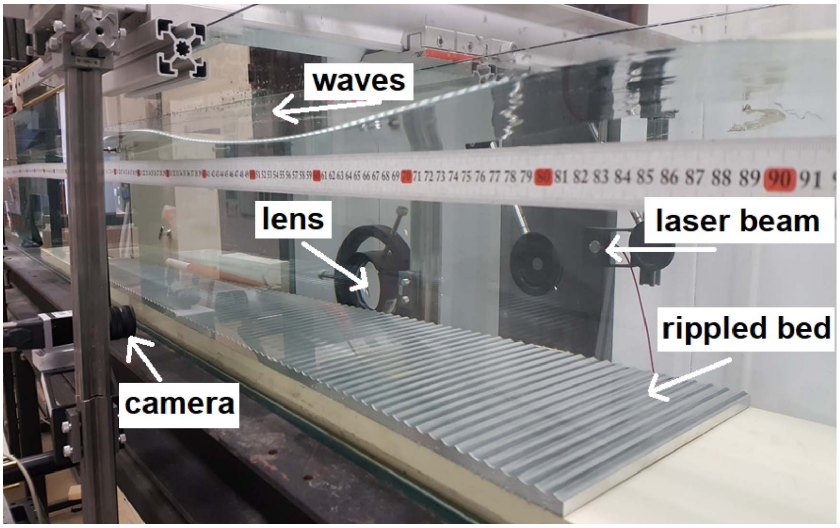

Figure 1. Photograph of the experimental set-up in the wave flume tank.

Table 1. Characteristics of the flow and the sedimentary transport for a median diameter d_{50} = 130 μm

	H_r (mm)	L_r (mm)	T (s)	H (mm)	λ (m)	U_∞ (m/s)	a (mm)
Test 1	1.7	11.5	0.7	30	0.72	0.048	5.4
Test 2	2.9	18.3	1.1	30	1.37	0.081	14.27
Test 3	4.1	24.9	1.5	30	1.98	0.092	22.06
	k_s (mm)	Re	f_{wL}–f_{wT}	ψ	θ_L–θ_T	θ_{cr}	
Test 1	6.28	262	0.12–0.26	5.27	0.33–0.67	0.09	
Test 2	11.49	1163	0.06–0.34	14.86	0.44–2.55	0.30	
Test 3	16.88	2038	0.04–0.33	19.13	0.42–3.13	0.30	

taken from Nielsen [1], the wavelength's formula takes into account the mobility number for d_{50} = 130 μm and the Reynolds number (defined later on). Thus, each ripple bed corresponds to the equilibrium state of sedimentary ripples for each tested wave conditions and a median diameter sediment d_{50} = 130 μm. The fixed rippled beds are 1 m length and have a thickness of 7 mm. The length of the fixed rippled beds is constrained by the engine used to machine the plates. The experimental set-up is illustrated in Figure 1.

Spherical Polyvinyl Chloride (PVC) grains of density ρ_s = 1350 kg·m^{-3} are used. A particle sieving is performed and five sets of particle sizes are identified as follows: fine particles with d_{50} = [63–80] μm, medium fine with d_{50} = [80–100] μm, medium with d_{50} = [100–125] μm, medium coarse with d_{50} = [125–160] μm and coarse particles with d_{50} = [160–200] μm.

The study is conducted with heterogeneous particles taking 20% by mass of each of the five sets of particles.

The preparation of the mixture of water and particles is carried out as follows. Particles are poured into a beaker with a few drops of hydrophilic liquid and water to prevent coalescence of the particles. The mixture is strongly stirred for a few minutes by removing the foam from the surface as it goes. Once the mixture is done, we let the particles at rest for a few minutes. Once the waves are established in the wave flume tank, the particles are then dropped with a pipette at

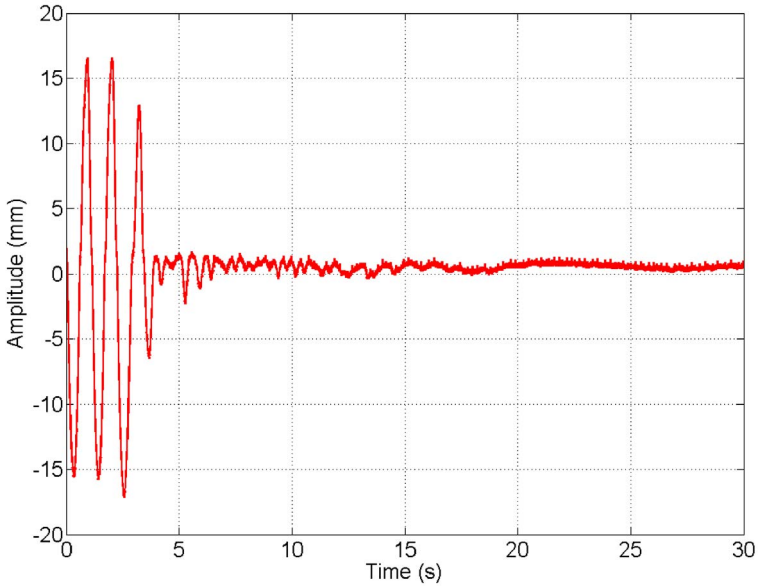

Figure 2. Wave damping signal. $t = 0$ corresponds to the stop of the wave maker.

the wave surface following the procedure of [11]. The particles are injected in the middle of the flume at 15 cm from the flume wall above the visualization area. The wavemaker is stopped at the beginning of the particle injection. Particles will then deposit under decreasing waves action. The wave damping time, defined as the time at which the wave amplitude is decreased by 85%, is about 4 s. Figure 2 presents the wave damping signal. The time $t = 0$ corresponds to the stopping of the wavemaker. As shown in the figure, the wave damping time takes a value of nearly 4 s. The particles reach the rippled bed before the complete damping of the free surface.

The sedimentation time of each range of size may be estimated using the Stokes velocity:

$$V_{\text{Stokes}} = \frac{2r^2 g \Delta\rho}{9\mu} \tag{2}$$

where g is the gravity acceleration, r is the radius of particle, $\Delta\rho = \rho_s - \rho$ the difference between the density of the particles ρ_s and the density of the fluid ρ, μ is the dynamic viscosity of water. For a water depth of 0.2 m, the sedimentation time varies between 26 s for the largest particles to 264 s for the smallest ones. However, the first particles are observed in the visualization area at about 7 s after injection and most of the particles reach the visualization area between 30 and 65 s.

2.2. *Flow conditions*

Fluid particles velocity at the bottom is given by $U_\infty = a\omega = \pi H/[T \sinh(kh)]$ where a is the orbital amplitude of fluid particles at the same place, $\omega = 2\pi/T$ the wave frequency, k the wavenumber and H the wave height. The Reynolds number is thus defined as $Re = U_\infty a/\nu$, with $\nu = 10^{-6}$ m^2·s^{-1} the water kinematic viscosity. The edge of the wave boundary layer is estimated to be located at one height k_s above the level midway between crest and trough of the ripples [17], where k_s is the Nikuradse roughness length, which may be estimated for a rippled bed by $k_s = 25H_r^2/L_r$. The Shields number θ is estimated as $\theta = 0.5 f_w \psi$, where f_w is the friction factor and $\psi = (a\omega)^2/[d_{50} \cdot g(s-1)]$ the mobility number with $s = \rho_s/\rho$, g the gravity

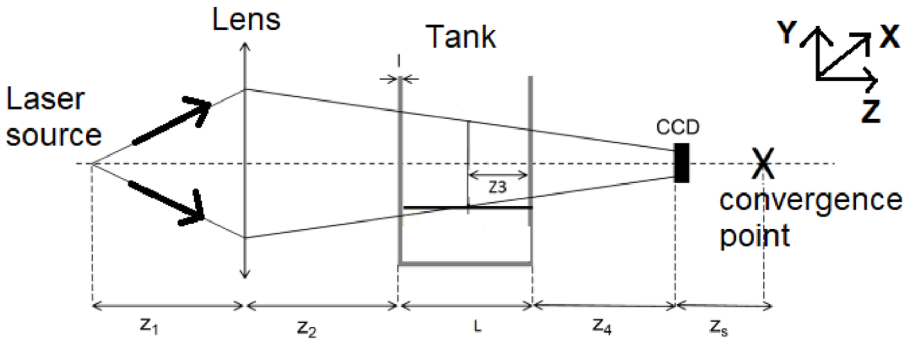

Figure 3. Scheme of the optical device. $L = 30$ cm, $l = 1$ cm, $z_1 = 41.5$ cm, $z_2 = 9$ cm, $z_4 = 8.5$ cm.

and $\rho = 1000$ kg·m^{-3} the water density. The flow regime is transitional, thus the friction factor may be defined as $f_w = 2/\sqrt{Re}$ for laminar flows and $f_w = \exp[5.213((2.5d_{50})/a)^{0.194} - 5.977]$ for rough turbulent flows [19]. All these parameters were obtained from calculation and not from measurements. The characteristics of the three rippled beds and the flow are presented in Table 1.

Following Davies [20], the flow regime depends on the values of Re and a/k_s. In our case, this regime is transitional between laminar and turbulent flow regime. Various expressions have been given to define the critical Shields number leading to the motion of particles. For small D_*, the more restrictive one is given by Soulsby *et al.* [21], where:

$$D_* = \left(\frac{g(s-1)}{\nu^2}\right)^{1/3} d_{50}.$$

In our experiments, the Shields number, before waves are stopped, in either laminar or turbulent flow conditions, is always larger than the critical Shields θ_{cr} leading to the motion of the particles.

2.3. *DIH calibration*

DIH is performed using a modulated fiber laser diode emitting a coherent light at the wavelength 640 nm and holograms are recorded by a lensless CCD camera Basler aca2040. The sensor is 2000×2000 pixels^2 with 5.5 μm square pixels so that the hologram size is 11×11 mm^2 which corresponds to 0.96 to $0.44\,L_r$. A convergent lens (focal length 350 mm) is placed between the optical fiber head and the flume to illuminate the sample volume with a convergent beam in order to increase the visualization area. The distance between the visualization area and the wave maker is 5.3 m. A scheme of the optical device is illustrated in Figure 3.

For more details on the DIH configuration, see Lebon *et al.* [22]. In order to find the correspondence between the coordinates of holographic images and the actual coordinates of particle in the tank, a calibration is needed. A square test pattern of concentric squares of dimension ranging from 2 mm to 10 mm with steps of 2 mm is placed in the sample volume in the middle of the flume (see Figure 4 left). The pattern is then shifted along z axis (optical axis) on 8 intervals with calibrated steps of 2 mm (se Figure 3 where z_3 denotes the distance between the channel intern wall and the square pattern). The motion of the square pattern is controlled by a linear translation stage equipped with a millimeter screw giving an accuracy of 0.1 mm on the mechanical motion of the pattern. A hologram is recorded for each position of the square pattern. For each hologram, the reconstruction depth plane that leads to the best focused image pattern is searched. Thus, the reconstruction distance z_r for each of the 8 positions is then obtained.

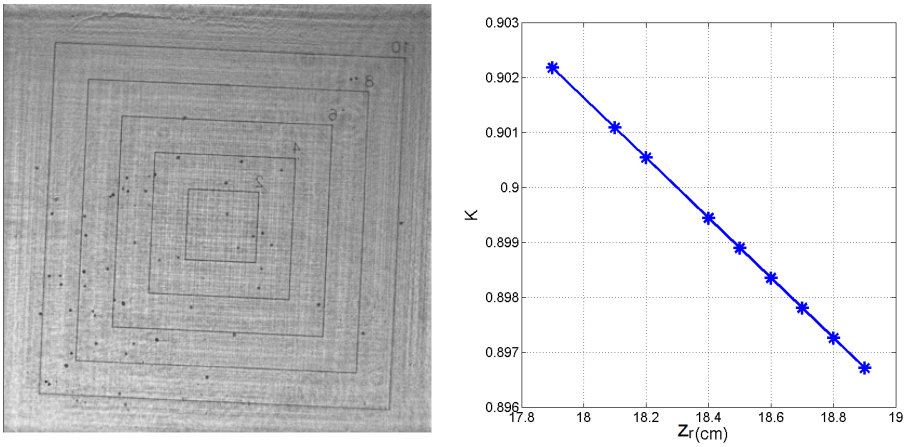

Figure 4. Left: The square pattern used for calibration. Right: Magnification factor K as function of the reconstructed axial distance Z_r.

However, the different propagation media crossed by the laser beam have to be taken into account, since a change of medium affects the optical path length of the wave. The magnification factor K is then expressed as follows:

$$K(z_r) = \frac{z_r}{z_e} \tag{3}$$

where $z_e = z_3 / n_{\text{water}} + l / n_{\text{glass}} + z_4$ is the equivalent geometric theoretical distance (Figure 3).

The magnification factor K is expressed as a function of the beam curvature radius z_s which is defined as the distance between the CCD sensor and the laser beam convergence point [23]. Then we obtain:

$$K(z_r) = \frac{z_s}{z_s - z_e} = \frac{z_s + z_r}{z_s}. \tag{4}$$

This formulation enables to express z_e as a function of z_r independently of $K(z_r)$:

$$z_e = \frac{1}{\frac{1}{z_s} + \frac{1}{z_r}}. \tag{5}$$

By plotting the calibrated value of z_e obtained by moving the square pattern, as function of the estimated value of z_e using relation (3), the value of z_s can be adjusted assuming a linear regression. A first estimated value of z_s is found. Then the value of z_s that leads to a straight line of slope equal to 1 is searched by dichotomy. K is finally determined as a function of z_e and z_s using relation (3). The result of the calibration is presented in Figure 3. The evolution of the magnification as a function of z_r is linear. We can thus extrapolate its value for any value of z_r using relation (3).

2.4. *3D particles coordinates*

The holograms are restored plane by plane for reconstruction distances z_r ranging from 80 mm to 310 mm by 1 mm intervals. This depth range corresponds to the whole width of the flume (i.e. 300 mm). In order to find the 3D particles coordinates, the hologram is then subdivided into regions of interest (ROI) crossing all the reconstructed planes. The size of the ROI must be carefully chosen in order to include the particles to be characterized. In our case, the maximum size of the particles is 200 µm (i.e. ~36 pixels). A ROI of 37×37 pixels^2 is therefore well suited. The detection algorithm searches for the reconstruction distance z_r that leads to the minimum light intensity for each ROI through the restored planes when the beam is obstructed by the particle.

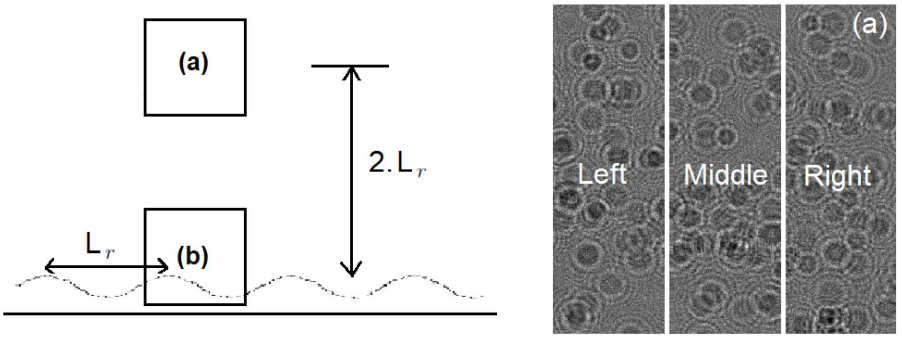

Figure 5. Left: Schematic representation of the two measurements zones (a) at two ripple wavelengths above the rippled bed (a) and at the rippled bed (b). Right: Example of a hologram in zone (a) at 36.6 mm above the rippled bed.

In other words, the z_r coordinate is identified by a minimum on the gray level profile. The image is then binarized. The threshold gray level is defined as the mean value between the background gray level and the minimum gray level in the ROI. At this stage, only dark objects are still present in the ROI. The method then consists in adjusting the equation of a circle to the selected particle candidate to determine its diameter. Its center is defined as the centroid of the remaining spot [24]. A SNR (Signal-to-Noise Ratio) of 7 dB is considered the minimum acceptable to separate a detection from an artifact. If this criterion is satisfied, the location at (x_h, y_h) and the diameter of the particle are estimated. The ROI is then recentered on its position. The expected accuracy on the estimation of depth coordinate (z_e) is of the order of a hundred micrometers [22].

The particle coordinates (x, y, z) are estimated from the particle image coordinates (x_h, y_h, z_r) obtained from the reconstructed hologram with the following equations:

$$\begin{cases} x = p\dfrac{x_h}{K(z_r)} \\ y = p\dfrac{y_h}{K(z_r)} \\ z = n_w\left(\dfrac{z_r}{K(z_r)} - \dfrac{z_{rp}(x_h)}{K(z_{rp}(x_h))}\right) \end{cases} \tag{6}$$

where $n_w = 1.33$ is the refractive index of water, $p = 5.5$ µm the pixel size and $z_{rp} = 84$ mm the reconstructed axial coordinate of the channel's inner wall, estimated during the calibration.

3. Experimental results

The aim of this study is to characterize the sorting of particles according to their size above three fixed rippled beds during wave damping phase. Measurements are performed in a visualization area above the rippled bed, including more than a half wavelength, except for Test 3. Three zones are then defined: above ripple crest, above ripple trough and an intermediate zone between ripple crest and trough.

However, in order to determine if any sorting of the particles occurs before reaching the rippled bed, a preliminary test is performed at 36.6 mm above the rippled bed, corresponding to two ripple wavelengths for Test 2 (see Figure 5). The choice of the two ripple wavelengths above the rippled bed is motivated by the assumption that above at least one wavelength from the ripples, the particles motion is no longer influenced by the vortices created in the vicinity

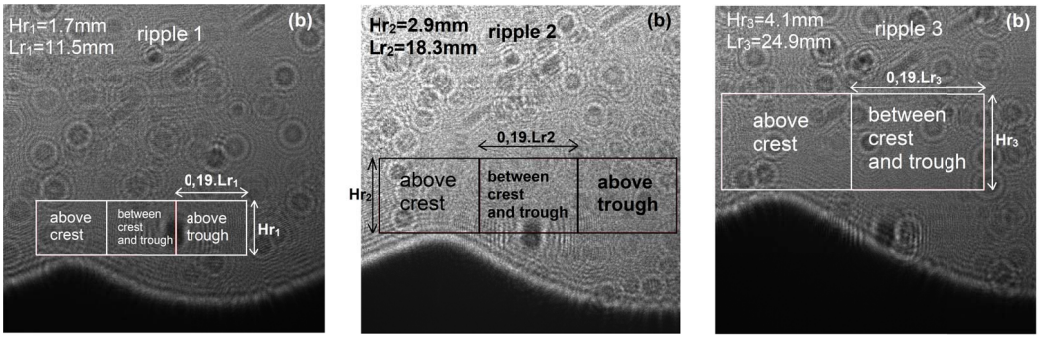

Figure 6. Example of holograms recorded just above the rippled bed, zone (b), for the three rippled beds.

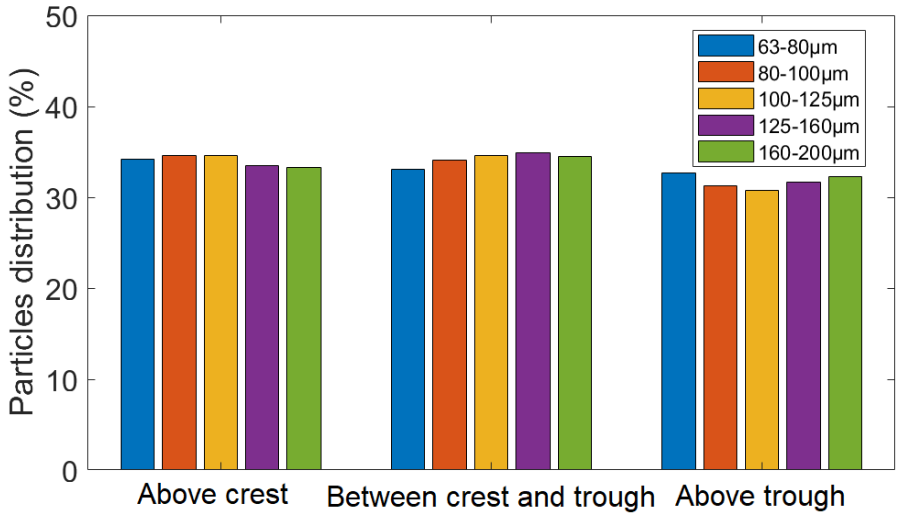

Figure 7. Distribution of heterogeneous particles at a distance of $2 \cdot L_r$ above the rippled bed 2.

of ripples [25]. The recording frequency in this case is 1 Hz. Each hologram is divided into three zones: left, middle, right (Figure 5 right).

For measurements above the rippled beds, the height of each zone corresponds to the ripple height and the length of the zone corresponds to 19% of the wavelength ripple (Figure 6) such that the half of a ripple wavelength is covered.

3.1. *Two ripple wavelength above the rippled bed*

In this section, the results are presented in terms of particles distribution above the rippled bed 2 ($H_r = 2.9$ mm; $L_r = 18.3$ mm). Heterogeneous particles are considered.

Figure 7 shows the heterogeneous particles distribution located at two ripple wavelengths above the rippled bed 2. For each range of particle size, the distribution is calculated as the total number of particles measured in each zone during 15 s. This number is normalized by the total number of particles of each range in the three zones.

According to the Figure 7, the particles of each range size are homogeneously distributed in the three zones with less than 2% of difference between the different zones. No surface sorting is observed. Following this result, we can now go further and characterize the particles concentration and distribution in the vicinity of the rippled bed.

3.2. *Measurements at the rippled bed*

In order to measure long time particles concentration evolution, the recording rate of holograms is set to 1 Hz for a total recording time of 450 s. This duration has been chosen as a satisfying compromise between sufficiently large recording time for all particles to be deposited and a uselessly long time. This recording time corresponds to 643 wave periods for the smallest wave periods and 280 wave periods for the largest wave periods, $T = 1.6$ s.

The volume particles concentration $C(t)$ is calculated in each of the three zones, with n the detected particles number at each time step and V the volume of each zone which sweeps the entire width of the channel along z axis:

$$C(t) = \frac{\sum_{i=1}^{n}(4/3\pi r_i^3)}{V} \tag{7}$$

with r_i the radius of each particle. Since 20% by mass of each class of particles are injected, the small particles are more numerous than the larger ones.

Figure 8 shows the temporal evolution of the concentration of heterogeneous particles located at the vicinity of the rippled bed. The abscissa corresponds to the dimensionless time t. The starting time $t = 0$ s is set simultaneously when the particles are injected at the free surface and the wavemaker is stopped. The minimum value of concentration corresponds to the concentration of one particle in the zone.

For all configurations, a first large peak of concentration is observed at about 50 s corresponding to the falling time of most particles considering the decreasing motion of waves. Then, due to large wavelengths motion, particles concentration oscillates till vanishing for the smallest particles. The concentration of the largest particles only undergoes oscillations above the trough of ripple 2 and in the intermediate zone of ripple 3. We do not identify coarse particles larger than 125 μm in these zones, they may have fallen elsewhere.

For the ripple 1, the peak of concentration is slightly more important above trough for the three smallest classes of particles. Then the concentration of the medium fine particles increases above crest. For the ripple 2, we can see that the particle concentration is higher above trough in comparison with the concentration above crest and between crest and trough. For the ripple 3, the visualization area is too small to observe the zone above trough. For this ripple, the concentration is almost the same between the two zones above crest and between crest and trough. For all ripples, the concentration never totally vanishes since at least one particle remains in the zone.

Those results are confirmed when looking at the particles distribution in the different zones for the three ripples represented in Figure 9. Fine particles distribution is larger above trough for the ripple 1 and ripple 2, comparing with the two others zones.

3.3. *Particle trajectories during wave damping*

Figure 10 presents the temporal evolution of the 3D particles coordinates of all the detected particles for the three rippled beds in the whole visualization area. The X coordinates stands for wave propagation direction, the Y coordinate is the vertical and Z is the coordinate along the flume width.

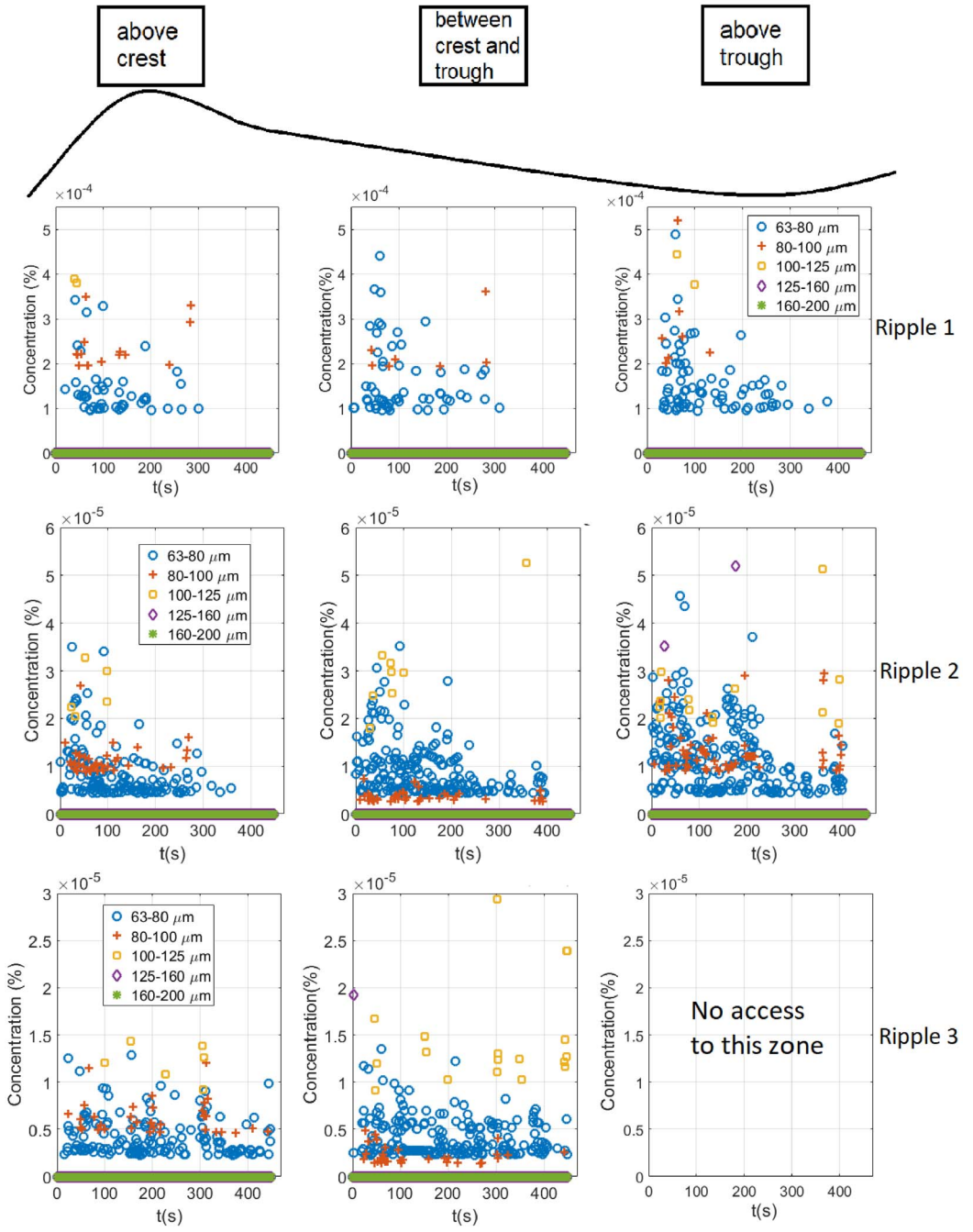

Figure 8. Temporal evolution of heterogeneous particle concentrations in the vicinity of the three rippled beds.

For the evolution in X and Y of ripple 1 and 2, we observe that the particles smaller than 125 μm are spread over all the zones up to about 300 s. Beyond this value, fewer particles are observed as they settle down. The drop of particles can be observed when looking at the evolution of Y coordinate with time.

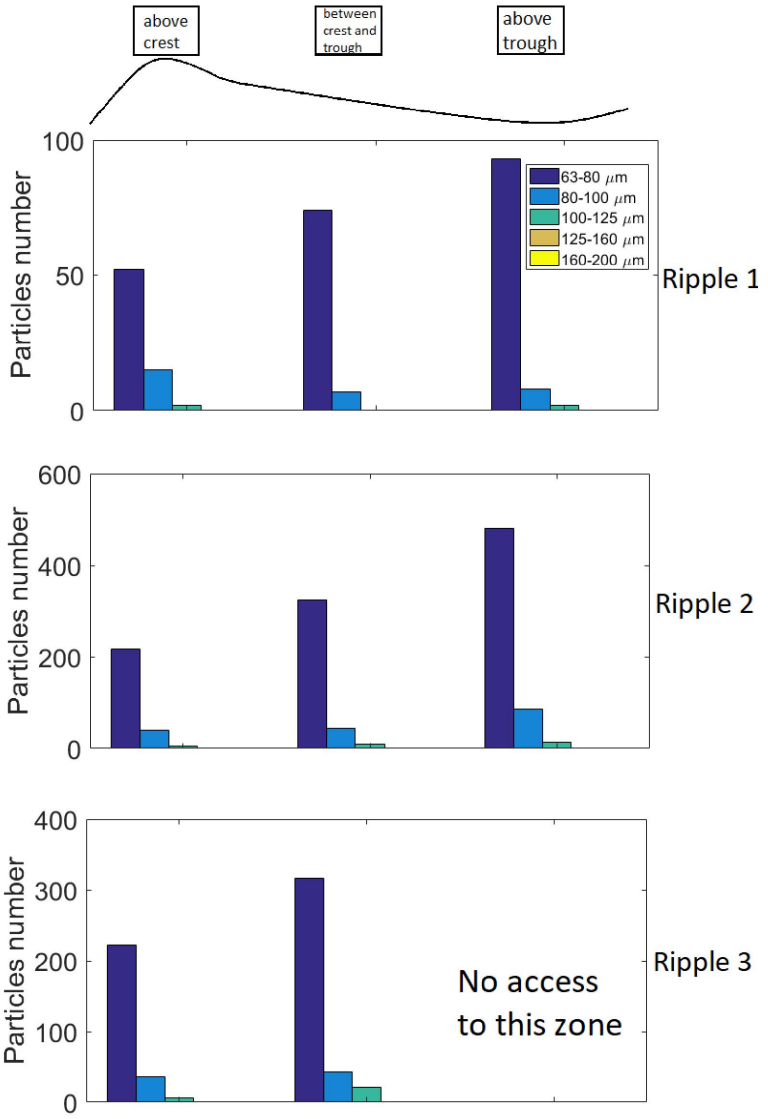

Figure 9. Particles number in the vicinity of the three rippled beds.

For ripple 2, as the particles settle down, they tend to move toward the crest. Indeed, the X position of particles increase as the time increases.

For the Z evolution, the particles are also spread over the entire width of the channel till they reach the visualization area. However, as time increases, 3D movements advect the particles towards the center of the flume particularly for ripple 1 and 2. Indeed, less particles are visible close to the flume wall. These motions may be due to transverse modes in the flume or to z-axis vortices formed at the ripple crests. Those vortices are connected to the flume's walls and thus induces z-axis velocities advecting particles toward the center of the flume. Regarding the ripple 3 and because of the high wave condition, particles are still in suspension after 400 s.

3D trajectories of three particles during sedimentation on a ripple crest and a ripple trough are determined by tracking each particle on thirty holograms recorded at 30 Hz. The measured

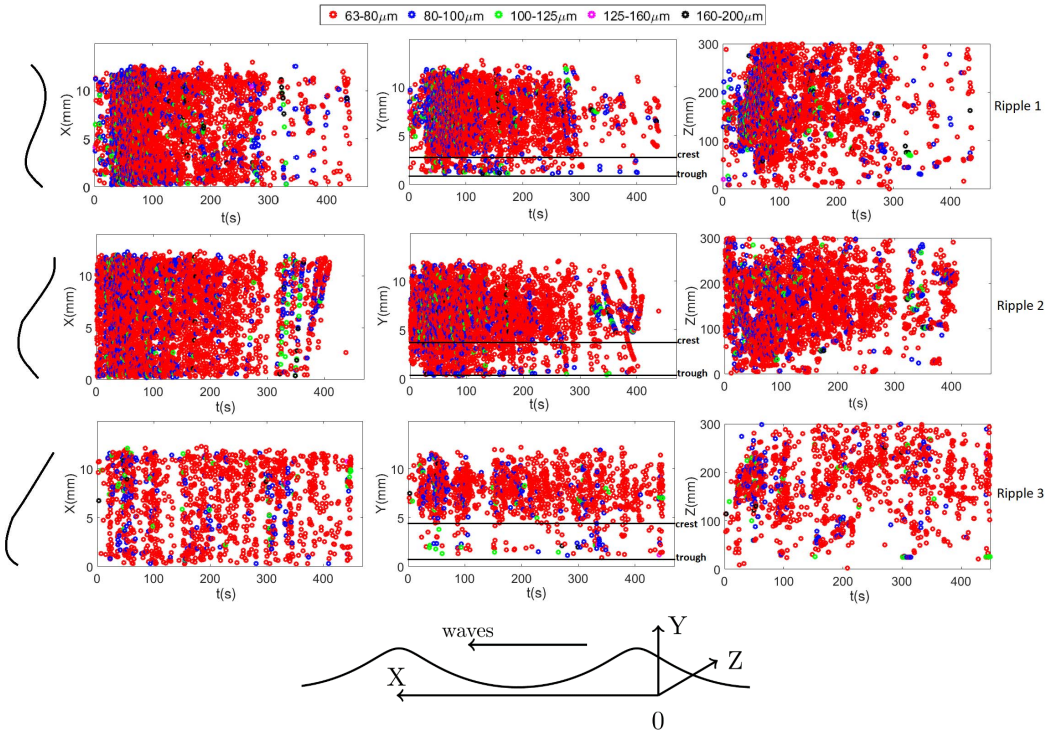

Figure 10. Temporal evolution of 3D particles coordinates in the vicinity of the three rippled beds.

diameters for particles above crest are 115 μm, 88 μm and 72 μm. As seen in Figure 11, the motion amplitude of the coarse particle is tighter than that of the two other particles. On the other hand, the diameters of the two detected particles above ripple trough are 70 μm and 107 μm. The motion amplitude of the finest particle is largest than the coarse particle.

Few studies have been dedicated to sediment size distribution over ripples in the field. The results of this study, in which the distribution of fine particles is larger above trough, were similar to the observations made by Foti *et al.* [9], Doucette [10], Noda *et al.* [26], De Best *et al.* [27] and Carter *et al.* [28].

Clifton *et al.* [29] found fine grains on ripple crest and coarse grains on ripple troughs. When the surface waves damp, Chu *et al.* [11] found fine particles concentrate on the top of ripple crests forming narrow strips, while coarse particles settle more uniformly along the rippled bed.

Miller *et al.* [30] found no difference in the grain size distributions between ripple crests and troughs. Their measurements were in either well sorted fine or medium grained sands. It is possible that the sand was too well sorted for there to be a significant difference in sediment sizes in crest and troughs.

The differences in particle size distribution between the ripple crests and troughs show the selectivity of transport over ripples. Similar particle sizes could be present in both crests and troughs, but they occurred in different abundances. This particle distribution depends on the particles sorting, on the geometry of the ripples and on the hydrodynamic flow field at the bottom.

This experimental study allows a global 3D visualization and characterization of the particles over fixed rippled beds compared to all previous studies performed in 2D for which we do not have access to the transverse behaviour of the particles.

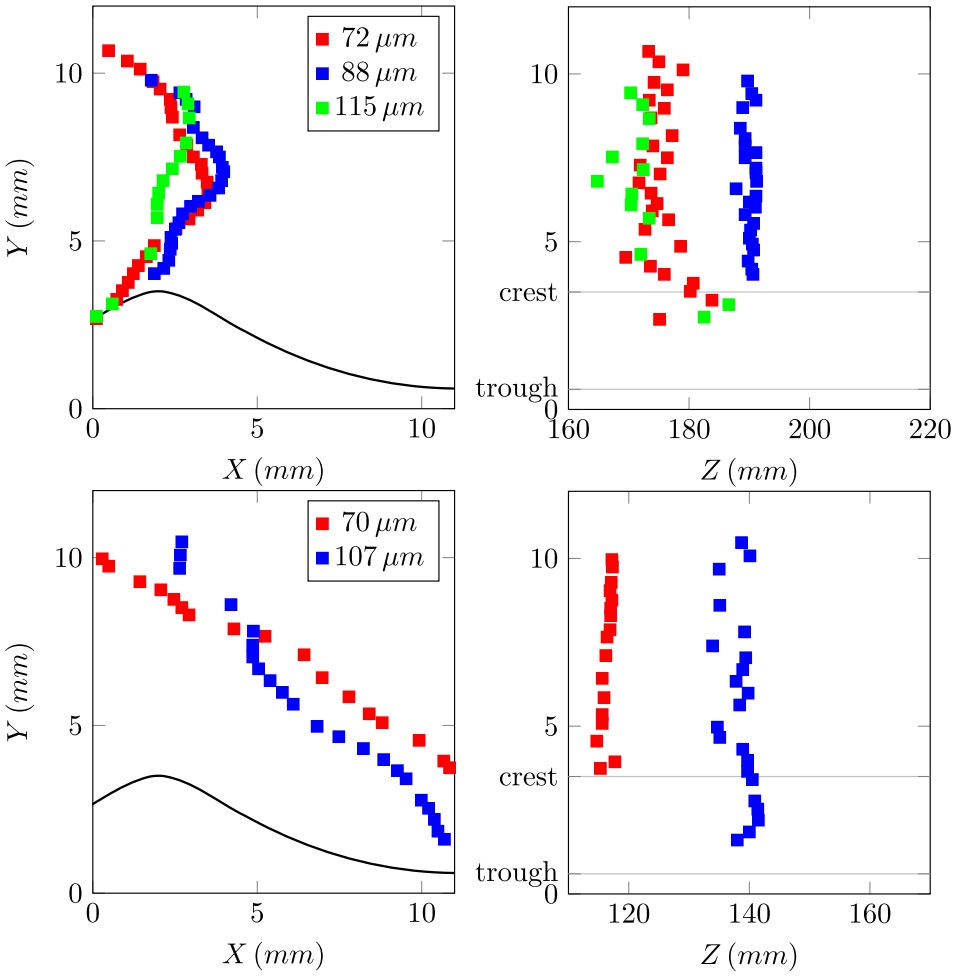

Figure 11. Top: Three particle trajectories above ripple crest. Bottom: two particle trajectories above ripple trough.

4. Conclusion

Measurement campaigns are conducted in a wave flume tank to study the particles motion over fixed rippled beds by digital in-line holography. The concentrations and distribution of particles in the three dimensions of space are obtained for heterogeneous particles in size.

Two areas are considered for measurements. The first one is located at two ripple wavelengths above the rippled bed and the second one is located in the vicinity of the ripples. For the first area, the results show that the temporal evolution of particles concentration is almost the same along x-direction for each range of particle size. This result confirms that the particle injection process is done homogeneously along x.

Regarding the measurements at the vicinity of ripples, the results show that the distribution of fine particles is larger above trough as shown in previous studies of Foti *et al.* [9] and Doucette [10]. However, no particular sorting is observed between the three first classes of particles in size. Due to the weak number of coarser particles, their identification is difficult and at least no particles are observed.

3D particles trajectories are studied above ripple crest and trough during wave damping. It is observed that the amplitude of motion of fine particle is larger than coarse particles. The coarse particles reach the rippled bed faster. The particles reach the rippled bed before the complete damping of the wave surface.

For our knowledge, all previous experimental studies on the particles distribution over rippled beds were in 2D. Using holography in such configuration is a great advantage. It allows to assess some particular interesting characteristics of particles in the three dimensions of space which is the particularity of this experimental study. Moreover, by recording a whole volume, holography technique enables to overcome the size measurement bias very classically observed in 2D imaging (i.e. the failure to take into account the the smallest defocused particle-images).

Even if scale effects are significant and the results in terms of particle motions and size are not the same in the wave flume tank and at real scale, this study allows the quantification of 3D particles concentration and distribution above a fixed rippled bed under waves.

The overall results provide an interesting complementary experimental database which could be used for the validation of future numerical models.

Conflicts of interest

Authors have no conflict of interest to declare.

Acknowledgements

This work is supported by the project of NEPTUNE. The authors would like to thank FEDER and the Normandie Regional Council for the financial funding of the project.

References

[1] P. Neilsen, "Dynamics and geometry of wave-generated ripples", *J. Geophys. Res.* **86** (1981), p. 6467-6472.

[2] J. Lebunetel-Levaslot, A. Jarno-Druaux, A. B. Ezersky, F. Marin, "Dynamics of propagating front into sand ripples under regular waves", *Phys. Rev. E* **82** (2010), article no. 032301.

[3] I. S. Aranson, L. S. Tsimring, "Patterns and collective behavior in granular media: Theoretical concepts", *Rev. Mod. Phys.* **78** (2010), p. 641-692.

[4] B. Stachurska, R. Staroszczyk, "An investigation of the velocity field over rippled sand bottom", in *6th International Junior Researcher and Engineer Workshop on Hydraulic Structures* (Lübeck, Germany), vol. 3, International Association for Hydro-Environment Engineering and Research, 2016.

[5] J. J. Van der Werf, "Sand transport over rippled beds in oscillatory flow", PhD Thesis, University of Twente, 2006, 206 pp.

[6] M. H. García, R. Musalem, D. M. Admiraal, "Exploratory study of oscillatory flow over a movable sediment bed with particle-image-velocimetry (PIV)", in *Hydraulic Measurements and Experimental Methods 2002*, American Society of Civil Engineers, Estes Park, CO, 2002, p. 711-720.

[7] P. Neilsen, "Suspended sediment concentrations under waves", *Coast. Eng.* **10** (1986), p. 23-31.

[8] P. Neilsen, *Coastal Bottom Boundary Layers and Sediment Transport*, World Scientific, Singapore, 1992, 340 p.

[9] E. Foti, P. Blondeaux, "Sea ripple formation: the heterogeneous sediment case", *Coast. Eng.* **25** (1995), p. 237-253.

[10] J. S. Doucette, "Geometry and grain-size sorting of ripples on low-energy sandy beaches: field observations and model predictions", *Sedimentology* **49** (2002), p. 483-503.

[11] T. D. Chu, A. Jarno-Druaux, F. Marin, A. B. Ezersky, "Particle trajectories and size sorting above a rippled bed under standing water waves", *Phys. Rev. E* **85** (2012), article no. 021304.

[12] P. Frank-Gilchrist, A. Penko, J. Calantoni, "Investigation of sand ripple dynamics with combined particle image and tracking velocimetry", *J. Atmos. Ocean. Technol.* **35** (2018), p. 2019-2036.

[13] J. R. Finn, M. Li, S. V. Apte, "Particle based modelling and simulation of natural and dynamics in the wave bottom boundary layer", *J. Fluid Mech.* **796** (2016), p. 340-385.

[14] E. A. Zedler, R. L. Street, "Sediment transport over ripples in oscillatory flow", *J. Hydraul. Eng.* **132** (2006), p. 180-193.

[15] K. J. Eidsvik, "Some contributions to the uncertainty of sediment transport predictions", *Cont. Shelf Res.* **24** (2004), p. 739-754.
[16] A. G. Davies, P. D. Thorne, "Modeling and measurement of sediment transport by waves in the vortex ripple regime", *J. Geophys. Res.* **110** (2005), article no. C05017.
[17] F. Marin, "Eddy viscosity and Eulerian drift over rippled beds in waves", *Coast. Eng.* **50** (2004), p. 139-159.
[18] J. Lebunetel-Levaslot, "Dynamique de formation des réseaux de rides de sable en canal à houle", Doctoral dissertation, Université du Havre, 2008.
[19] D. H. Swart, "Coastal sediment transport. Computation of longshore transport", 1976, Report R868 (1), Delft Hydraulics Laboratory.
[20] A. G. Davies, "Field observations of the threshold of sand motion in a transitional wave boundary layer", *Coast. Eng.* **4** (1980), p. 23-46.
[21] R. Soulsby, R. Whitehouse, "Threshold of sediment motion in coastal environment", in *Proceedings of the Pacific Coasts and Ports '97 Conference*, University of Canterbury, Christchurch, New Zealand, 1997, p. 149-154.
[22] B. Lebon, G. Perret, S. Coetmellec, G. Godard, G. Gréhan, D. Lebrun, J. Brossard, "A digital holography set-up for 3D vortex flow dynamics", *Exp. Fluids* **57** (2016), article no. 103.
[23] D. Lebrun, D. Allano, L. Mees, F. Walle, F. Corbin, R. Boucheron, D. Frechou, "Size measurement of bubbles in a cavitation tunnel by digital in-line holography", *Appl. Opt.* **50** (2011), no. 34, p. H1-H9.
[24] S. L. Pu, D. Allano, B. Patte-Rouland, M. Malek, D. Lebrun, K. F. Cen, "Particle field characterization by digital in-line holography: 3D location and sizing", *Exp. Fluids* **39** (2005), no. 1, p. 1-9.
[25] P. L.-F. Liu, K. A. Al-Banaa, E. A. Cowen, "Water wave induced boundary layer flows above a ripple bed", in *PIV and Water Waves*, World Scientific, Singapore, 2004.
[26] H. Noda, "A study on mass transport in boundary layers in standing waves", in *Proceedings of the 11th Coastal Engineering Conference* (London, UK), ACSE, 1968, p. 227-235.
[27] A. De Best, E. W. Bijker, "Scouring of a sand bed in front of a vertical breakwater", 1971, Communications on Hydraulics, Report 71-1. Department of Civil Engineering, Delft University of Technology, Delft, The Netherlands.
[28] T. G. Carter, P. L. F. Liu, C. C. Mei, "Mass transport by waves and offshore sand bedforms", *J. Waterw. Port Coast. Eng.* **99** (1973), p. 65-184.
[29] H. E. Clifton, R. E. Hunter, R. L. Phillips, "Depositional structures and processes in the non-barred highenergy nearshore", *J. Sed. Petrol.* **41** (1971), p. 651-670.
[30] M. C. Miller, P. D. Komar, "A field investigation of the relationship between oscillation ripple spacing and the near-bottom water orbital motions", *J. Sed. Petrol.* **50** (1980), p. 0183-0191.